International Journal of Innovation in Science and Mathematics
Volume 4, Issue 6, ISSN (Online): 2347–9051

Study on Highly Efficient Carrier Injection into Wide-bandgap Active Layers in Organic Light-emitting Diodes

Masato Osumi, Akira Matsuoka, and Naoki Ohtani
Department of Electronics, Doshisha University, Kyoto, Japan
ohtani@mail.doshisha.ac.jp

***Abstract* – Carrier transport properties in organic light-emitting diodes (OLEDs) containing wide-bandgap active layers were studied for application to ultraviolet light emitters. 3-(Biphenyl-4-yl)-5-(4-tert-butylphenyl)-4–phenyl-4H-1, 2, 4-triazole (TAZ) was used as an emissive material, whose emission wavelength is about 382 nm. The triple-layer structure samples in which TAZ was sandwiched by electron- and hole-transporting layers revealed the undesired longer wavelength emissions originating from the exciplex emissions. Consequently, we found that the quadruple-layer structure samples consisting of an intermediate hole-injection layer between TAZ and the hole-transporting layers can suppress the exciplex emissions. In addition, the external quantum efficiency was drastically improved by changing the material of the electron-transporting layer due to the improved electron injection and the hole-blocking effect leading to the large accumulation of holes in TAZ.**

***Keywords* – Organic Light-emitting Diode, Carrier Transport, Wide-bandgap, TAZ.**

I. INTRODUCTION

Since the innovation of organic light emitting diodes (OLEDs) [1], they have been energetically studied for application to novel flat panel displays [2-4] and illumination light sources [5-7], because OLEDs are expected to have advantages over inorganic LEDs, such as brightness, energy-saving, low-cost production, and flexibility. These studies focused on the OLEDs operating in the visible light regime. Recently, some studies on the fabrication of OLEDs operating in the ultraviolet regime have been performed [8, 9]. However, the observed external quantum efficiencies (η_{ex}) of them were 0.8%[8] and 3.1% [9]. These results were smaller than that of AlGaN-based LED [10], in which the η_{ex} of 10.4% was reported, nevertheless the emission wavelength was the deep-ultraviolet of 278 nm. The efficient carrier injection into wide-bandgap emissive materials ought to be difficult in both inorganic- and organic-LEDs. However, these results imply that the research on the carrier transport properties in OLEDs has been insufficient. In this study, we fabricated OLEDs consisting of the wide-bandgap active layer operating in the near ultraviolet regime. To improve the carrier injection into the active layer, triple- and quadruple-structure OLEDs consisting of electron- and hole-injection layers and an intermediate hole-injection layer were studied.

II. EXPERIMENTAL

A. Sample Fabrication

3-(Biphenyl-4-yl)-5- (4-tert-butylphenyl)- 4–phenyl-4H-1, 2, 4-triazole (TAZ) was used as an emissive material in the active layer, whose bandgap was about 3.9 eV. We confirmed that the emission wavelength of TAZ is in the ultraviolet regime of 382 nm by the photoluminescence (PL) measurement. 4, 4′, 4″-Tri (N-carbazolyl) triphenylamine (TCTA) and N, N‘-Di (1-naphthyl)-N, N‘-diphenylbenzidine (α-NPD) were used as hole-transporting materials, while the following three different materials, 2, 9-Dimethyl-4, 7-diphenyl-1, 10-phenanthroline (BCP), 4, 7-Diphenyl-1, 10-phenanthroline (Bphen), and (2, 2', 2"- (1, 3, 5-Benzinetriyl)-tris (1-phenyl-1- H-benzimidazole) (TPBi) were used as electron-transporting materials. In addition, a 4, 4-Bis(N-carbazolyl)-1, 1-biphenyl (CBP) was used as an intermediate hole-injection material to improve the hole-injection into the active layer. All organic layers were vacuum-deposited on indium-tin-oxide (ITO)-coated cleaned SiO_2 substrates [11]. Finally, aluminum (Al) and LiF were deposited as the cathode metal.

We fabricated the two kinds of OLEDs. Figure 1 shows the schematic illustrations of cross-sectional sample structures. The sample of Fig. 1(a) consists of three organic layers; the electron-transporting layer (ETL) of BCP, the active layer of TAZ, and the hole-transporting layer (HTL). We used α-NPD and TCTA as a HTL and compared their electroluminescence (EL) properties. On the other hand, the sample of Fig. 1(b) consists of four organic layers; the ETL, the active layer of TAZ, an intermediate hole-injection layer (IML) of CBP, and HTL of TCTA. We used BCP, Bphen and TPBi as an ETL and compared their EL properties. Consequently, we fabricated the following five samples,

A: ITO / α-NPD / TAZ /BCP/ LiF / Al,
B: ITO / TCTA / TAZ /BCP/ LiF / Al,
C: ITO / TCTA/ CBP / TAZ /BCP/ LiF / Al,
D: ITO / TCTA / CBP / TAZ / Bphen/ LiF / Al,
E: ITO / TCTA / CBP / TAZ / TPBi/ LiF / Al.

Samples A and B correspond to Fig. 1(a), while the other three samples correspond to Fig. 1(b).

B. Measurement Setup

The EL spectra and the η_{ex} were recorded using a multi-channel spectrometer (Hamamatsu Photonics PMA-12 C10027-02), a source meter (Keithley 2400) and an integrating sphere unit (Hamamatsu Photonics A10094). Current-voltage characteristics were measured using a

semiconductor parameter analyzer (Agilent 4155C). PL spectra were recorded using a multi-channel spectroscope (Ocean Optics USB-2000), and a pulsed N_2 laser was used to photoexcite the samples. All measurements were performed in the atmosphere and at room temperature.

III. Results and Discussion

A. PL Spectra of Seven Low-weight Molecular Materials

We used seven low-weight molecular materials as explained in 2.1. The observed EL spectra may reveal multi-peaking-wavelengths, because all the seven materials are emissive materials and the samples are triple- and quadruple-layer structures consisting of them. Thus, we have to know the emission wavelengths of the seven materials to assign the origin of the observed EL multi-peaking-wavelengths. Figure 2 shows PL spectra of the seven materials studied. In addition, all the observed PL peaking-wavelengths of the seven materials are listed in Table 1, extracted from the PL spectra shown in Fig. 2. The emission wavelength of TAZ was 382 nm, which is the shortest in this group.

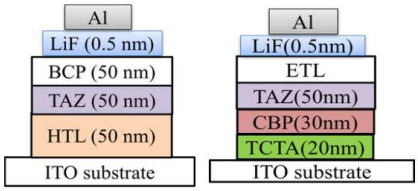

(a) (b)

Fig. 1. Schematic illustrations of cross-sectional sample structure. (a) consists of three organic layers, (b) consists of four organic layers.

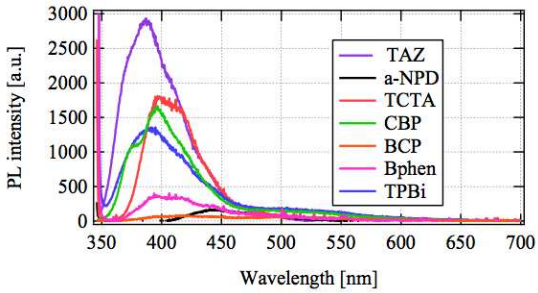

Fig. 2. PL spectra of materials studied.

Table 1. Observed PL peaking-wavelengths of the seven materials extracted from the PL spectra shown in Fig. 2.

	TAZ	a-NPD	TCTA	CBP	BCP	Bphen	TPBi
Peak (nm)	382	448	397	396	411	395	392

B. EL Properties of Samples A and B

Figure 3 shows EL spectra of samples A and B. The peaking-wavelength of sample A is about 440 nm, not corresponding to the emission of TAZ. On the other hand, EL spectrum of sample B reveals the peaking-wavelength at around 380 nm. This can be assigned to originate from the emission of TAZ. However, the EL spectrum of sample B reveals the undesired two peaking-wavelengths in the visible light regime. Moreover, their intensities are stronger than that of TAZ. To assign the origin of these emissions, we discuss the carrier transport properties in samples A and B on their energy band diagrams shown in Fig. 4. The most important difference among them is the discontinuity of Highest Occupied Molecular Orbital (HOMO) levels between TAZ and HTL. In the case of sample A, this discontinuity is about 1.2 eV, which is large enough to suppress the effective hole-injection into the active layer of TAZ as shown in Fig. 4(a). This leads to the large amount of radiative recombination in the HTL of α-NPD. Thus, the observed EL emission in sample A can be attributed to the emission from α-NPD.

In the case of sample B, the discontinuity of HOMO levels between TAZ and TCTA is about 0.9 eV, which is smaller than that of sample A. This means that some holes were injected into TAZ, leading to the ultraviolet emission at around 380 nm from TAZ. On the other hand, the undesired longer wavelength emissions in the visible light regime were most likely caused by the exciplex at the interface between TAZ and TCTA.

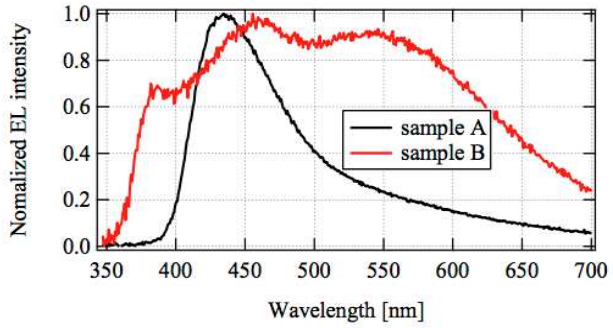

(b)

Fig. 3. Normalized EL spectra of samples A and B when the applied voltage is 12 V.

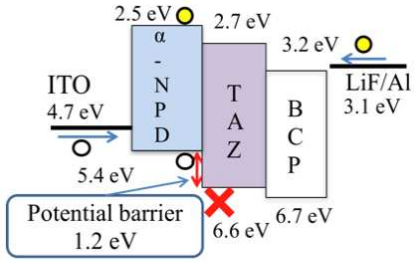

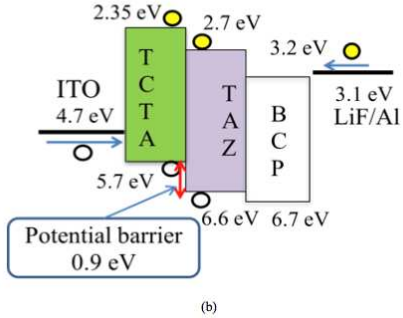

Fig. 4. Schematic illustrations of energy band diagrams of (a) sample A and (b) sample B.

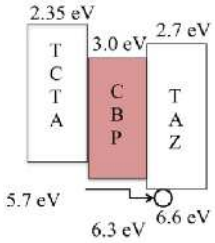

Fig. 5. Alignment of energy bands of TAZ, CBP, and TCTA in sample C.

C EL Properties of Sample C

To reduce the exciplex emissions of sample B, we used the IML of CBP between TAZ and TCTA to improve the hole-injection from TCTA to TAZ. The discontinuity of HOMO levels between TCTA and TAZ was expected to be reduced, because the HOMO level of CBP locates between TCTA and TAZ as shown in Fig. 5. The EL spectrum of sample C was shown in Fig. 6. It is very clear that the longer wavelength emissions observed in sample B were drastically reduced and the observed peaking-wavelength is only at around 380 nm. This result clearly indicates that the hole-injection into TAZ in sample C was drastically improved and the emission was caused only in the active layer of TAZ. However, the observed η_{ex} of sample C was about 0.1%.

The emission wavelength of sample C corresponds to the PL peaking-wavelength of TAZ. However, the emission from the adjacent CBP layer was not clearly observed, nevertheless the energy bandgap of CBP is narrower than that of TAZ as shown in Fig. 5. One possible cause is the large layer thickness of TAZ. The almost electrons injected to TAZ disappeared due to the radiative recombination in TAZ, because the thickness of TAZ is 50 nm; this is probably enough to consume the amount of injected electrons. Then, the remaining electrons were injected into the adjacent CPB layer, resulting in the weak emission. In addition, the thickness of CBP layer is 30 nm; this is thinner than TAZ, also leading to the weak emission from CBP. The PL peaking-wavelength of CBP is 396 nm (Table 1), which is close to the emission of TAZ. Thus, the weak EL emission from CBP may be screened by the strong emission from TAZ. Consequently, the main EL emission of sample C was caused in TAZ.

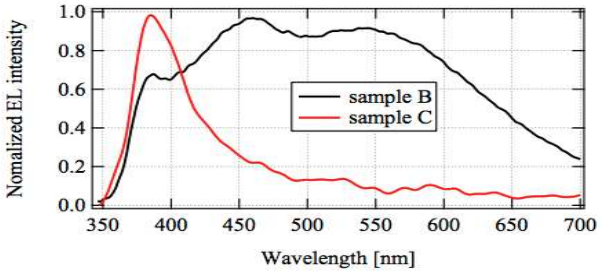

Fig. 6. Normalized EL spectra of samples B and C when the applied voltage is 12 V.

DEL Properties of Samples D and E

To improve the intensity of the ultraviolet emission from TAZ, we used Bphene and TPBi as ETL instead of BCP. Figure 7 shows EL spectra of the three samples C, D, and E when the applied voltage was 12 V. It is obvious that the emission intensity of about 380 nm originating from TAZ becomes the maximum in sample E (TPBi). The EL intensity of sample E is about ten times larger than the other two samples. Figure 8 (a) shows the current-voltage characteristics of them. The current injection of the three samples at 12 V is almost equal. Thus, the η_{ex} of sample E was also improved. Figure 8 (b) shows the η_{ex}–voltage characteristics of them. The observed η_{ex} of sample E was about 0.7% which is about seven times larger than other two samples. In this case, the luminance was 398 cd/m^2.

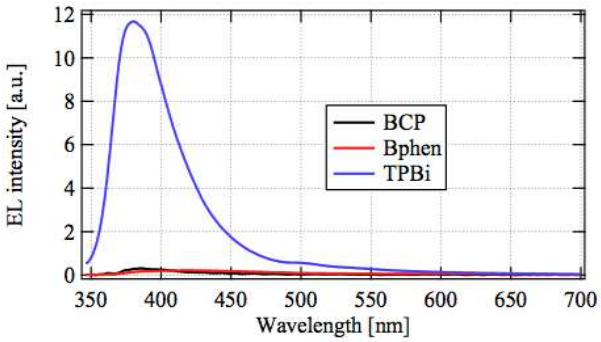

Fig. 7. EL spectra of samples C, D, and E when the applied voltage is 12 V.

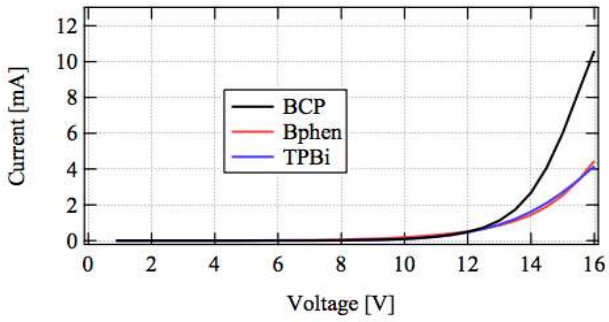

(a)

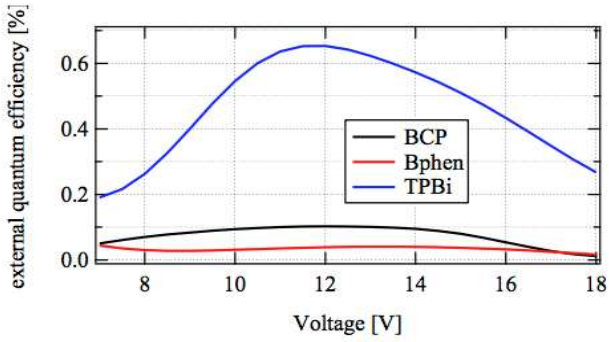

(b)

Fig. 8. (a) Current-voltage characteristics and (b) η_{ex}–voltage characteristics of samples C, D and E.

The energy band diagrams of samples D and E are shown in Fig. 9 to discuss the carrier transfer in both samples. The most important difference among them is the alignment of Lightest Unoccupied Molecular Orbital (LUMO) levels of TAZ and ETL. In sample D, the

discontinuity of LUMO levels between TAZ and Bphene is 0.3 V, by which some electrons were prevented to move to TAZ. On the other hand, the alignment of LUMO levels of TAZ and TPBi is equal in sample E. This means that the electron-injection into TAZ was not prevented. In addition, TPBi also works as a hole-blocking layer, because the HOMO level of TPBi locates below that of TAZ. This results in the accumulation of holes in TAZ as well as the large external quantum efficiency. On the other hand, the HOMO level of Bphene locates above that of TAZ as shown in Fig. 9. Thus, Bphene does not work as the hole-accumulation layer, resulting in the weak EL emission from TAZ. These results clearly indicate that the carrier injection into the wide-bandgap emissive layer was improved, resulting in the strong ultraviolet emission.

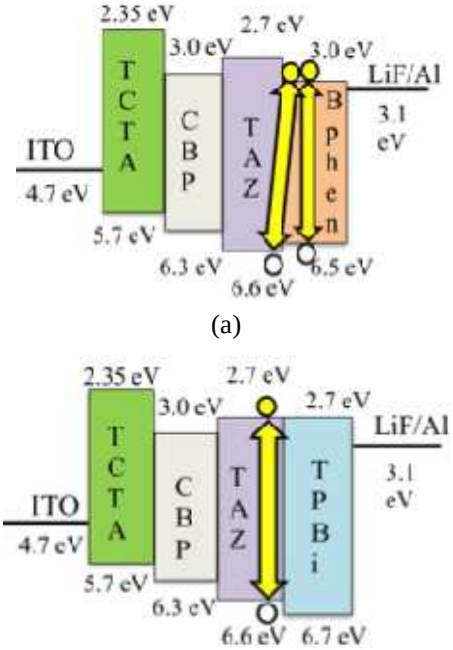

Fig. 9. Energy band diagrams of samples D and E. The yellow arrows indicate the radiative recombination paths between electrons and holes.

IV. Conclusion

High efficiently carrier injection into the wide-bandgap emissive material TAZ was realized by the discussion on the carrier transfer properties in multilayer OLEDs. To suppress the undesired emissions in the visible light regime, the intermediate hole-injection layer of CBP was introduced between the hole-transporting layer and the active layer. In addition, the electron-transporting layer of TPBi works also as a fine hole-blocking layer, resulting in the improved electron-injection and hole-accumulation in the active layer. Consequently, the external quantum efficiency was drastically improved. This demonstrates that high performance OLEDs operating in the ultraviolet regime were successfully fabricated.

Acknowledgment

This work was partially supported by a Grant-in-Aid for Scientific Research (Grant No. 25420348 and 16K06322) from the Japan Society for the Promotion of Science.

References

[1] C. W. Tang, and S. A. VanSlyke, “Organic electroluminescent diodes”, Appl. Phys. Lett., 51, pp.913-915 (1987).

[2] M. Slawinski, M. Weingarten, M. Heuken, A. Vescan, H. Kalisch, “Investigation of large-area OLED devise with various grid geometries”, Organic Electron. 14, pp. 2387-2391 (2013).

[3] M. Kimura, S. Imai, “Degradation evaluation of α-IGZO TFTs for application to AM-OLEDs”, IEEE Elec. Dev. Lett. 31, pp. 963-965 (2010).

[4] H. Kanno, Y. Hamada, H. Takahashi, “Development of OLED with high stability and luminance efficiency by co-doping methods for full color displays”, IEEE J. on Selected Topics in Quantum Elec. 10, pp. 30-36 (2004).

[5] M. Mesta, M. Carvelli, R. J. DeVries, H. Van Eersel, J. J. M. Van Der Holst, M. Schober, M. Furno, B. Lüssem, K. Leo, P. Loebl, R. Coehoorn, and P. A. Bobbert, “Molecular-scale simulation of electroluminescence in a multilayer white organic light-emitting diode”, Nature Materials, 12, pp. 652-658 (2013).

[6] C. Weichsel, L. Burtone, S. Reineke, S. I. Hintschich, M. C. Gather, K. Leo, and B. Lüssem, “Storage of charge carriers on emitter molecules in organic light-emitting diodes”, Phys. Rev. B, 86, 075204 (2012).

[7] M. Schober, M. Anderson, M. Thomschke, J. Widmer, M. Furno, R. Scholz, B. Lüssem, and K. Leo, “Quantitative description of charge-carrier transport in a white organic light-emitting diode”, Phys. Rev. B, 84, 165326 (2011).

[8] M. Ichikawa, K. Kobayashi, T. Koyama, and Y. Taniguchi, “Intense and efficient ultraviolet electroluminescence from organic light-emitting devices with fluorinated copper phthalocyanine as hole injection layer”, Thin Solid Films, 515, pp. 3932-3935 (2007).

[9] A. Mikami, Y. Mizuno, and S. Takeda, “High efficiency ultraviolet light emitting organic devices and its application to white light source”, Dig. of Tech. Papers –SID Int. Symp. 39, pp. 215-218 (2008).

[10] M. Shatalov, W. Sun, A. Lunev, X. Hu, A. Dobrinsky, Y. Bilenko, J. Yang, M. Shur, R. Gaska, C. Moe, G. Garrett, and M. Wraback, “278 nm deep ultraviolet LEDs with 11% external quantum efficiency”, Dev. Res. Conf. – Conf. Dig, DRC, 6257013, pp. 255-256 (2012).

[11] K. Kurata, K. Kashiwabara, K. Nakajima, Y. Mizoguchi, and N. Ohtani, “Time-of-flight measurement of hole-tunneling properties and emission color control in organic light-emitting diodes”, AIP conf. Proc. 1399, pp. 865-866 (2011).